Hindawi Publishing Corporation
Journal of Nanomaterials
Volume 2013, Article ID 640146, 7 pages
http://dx.doi.org/10.1155/2013/640146

Research Article

Synthesis of Octahedral-Shaped NiO and Approaches to an Anode Material of Manufactured Solid Oxide Fuel Cells Using the Decalcomania Method

Haeran Cho,[1] Huryul Lee,[2] Sun-Min Park,[1] Byung-Hyun Choi,[1] and Misook Kang[2]

[1] *Korean Institutes of Ceramic Engineering & Technology (KICET), Geumcheon-gu, Seoul 153-801, Republic of Korea*
[2] *Department of Chemistry, College of Science, Yeungnam University, Gyeongsan, Gyeongbuk 712-749, Republic of Korea*

Correspondence should be addressed to Misook Kang; mskang@ynu.ac.kr

Received 30 November 2012; Revised 25 February 2013; Accepted 17 March 2013

Academic Editor: Jie-Fang Zhu

Micrometer-sized and octahedral-shaped NiO particles were synthesized by microwave thermal treatment at 300 watt power for 15 min in a microwave chamber to be used as an anode material in solid oxide fuel cells. SEM image and particle size distribution revealed near-perfect octahedral NiO microparticle with sizes ranging from 4.0~11.0 μm. The anode functional layer (AFL, 60 wt% NiO synthesized: commercial 40 wt% YSZ), electrolyte (commercial Yttria-stabilized zirconia, YSZ), and cathode (commercial $La_{0.8}Sr_{0.2}MnO_3$, LSM) layers were manufactured using the decalcomania method on a porous anode support, sequentially. The sintered electrolyte at 1450°C for 2 h using the decalcomania method was dense and had a thickness of about 10 μm. The cathode was sintered at 1250°C for 2 h, and it was porous. Using humidified hydrogen as a fuel, a coin cell with a 15 μm thick anode functional layer exhibited maximum power densities of 0.28, 0.38, and 0.65 W/cm^2 at 700, 750, and 800°C, respectively. Otherwise, when a commercial YSZ anode functional layer was used, the maximum power density was 0.55 W/cm^2 at 800°C.

1. Introduction

Solid oxide fuel cells (SOFCs) consist entirely of metal oxides, NiO, YSZ, and LSM and have advantages of high efficiency and durability without expensive catalysts. However, it is difficult to control the size and shape of the ceramics produced because of many restrictions and complex geometries. In order to solve these problems, many researchers have studied means of maximizing reaction areas by changing stack sizes and developing new materials [1–5]. In many of these areas, SOFC fabrication methods are generally considered to be limiting factors based on considerations of automation and scalability [6]. Some SOFC structures are produced using traditional ceramic preparation methods, such as powder pressing, tape casting, screen printing, or conventional spray methods [7]. Other more sophisticated methods, such as plasma spraying [8, 9], vacuum deposition [10], and extrusion-based direct-write methods [11], have also been reported. Here, the decalcomania printing method is introduced. This method involves the transfer of designs from specially prepared paper to a wood or glass or metal surface. This method is expected to have some advantages because it is easy to prepare materials of the desired shape and size; manufacturing is straightforward. On the other hand, NiO/YSZ is widely used as an anode material for SOFCs because it has sufficient electronic conductivity and a good catalytic reaction for fuel gas at its operating temperature. Generally, anode materials for SOFCs also should be thermally and chemically compatible compared with other component materials at operating and higher temperatures, because SOFCs operate in the temperature range 800~1000°C. However, commercial NiO-loaded YSZ anode materials have a serious problem, because they are strongly deactivated during the operations of SOFCs, because of NiO aggregation at high temperature. Research into the synthesis of NiO nanoparticles has increased during the past decade and methods such as, sol-gel [12], microemulsion precipitation [13], chemical vapor deposition [14], and sputtering [15] have been designed. Recently, some researchers [16] have attempted to use advanced microwave treatments

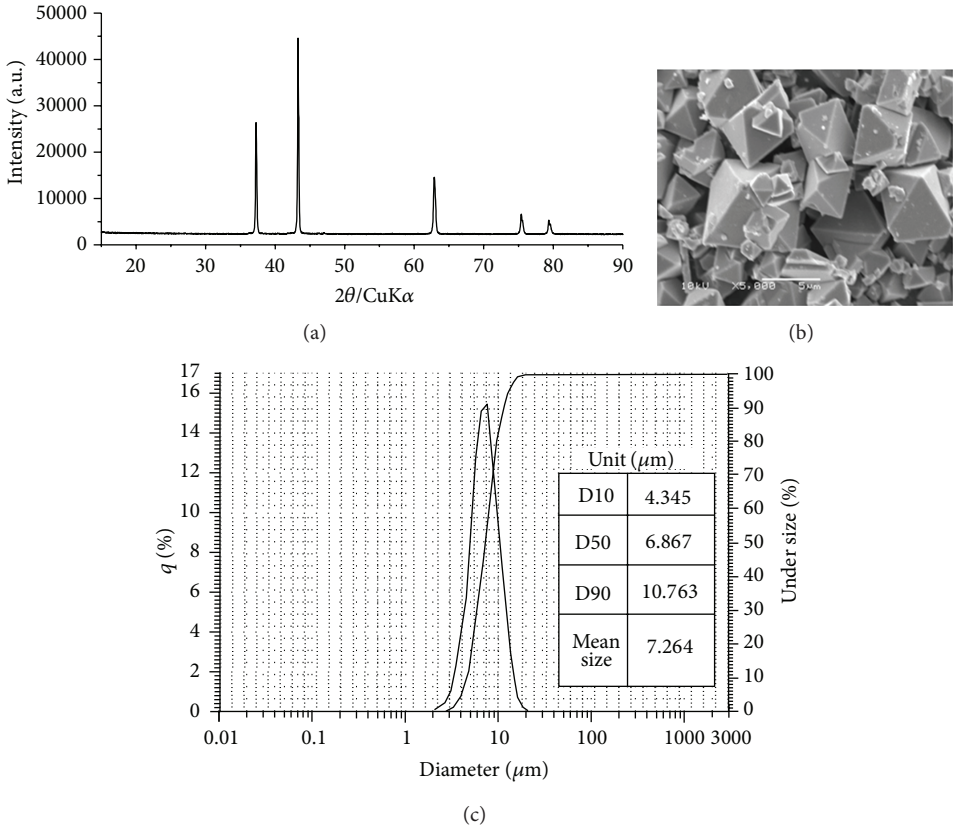

Figure 1: XRD pattern (a), SEM image (b), and particle size distribution (c) of the NiO powder synthesized using the microwave thermal treatment.

using various polymeric or surfactant additives to synthesize various metal materials with special morphologies. However, few studies have addressed the morphology for NiO as an anode material for SOFCs [17, 18]. In this study, we examined the preparation of microsized octahedral NiO particles using a microwave thermal treatment. Microwave heating was found to increase densification and shortened sintering time as compared with conventional heating. The synthesized NiO was characterized by X-ray diffraction (XRD), transmission electron microscopy (SEM), particle size, and zeta potentials. In order to explore the applicability of decalcomania printing to SOFC materials, a traditional set of SOFC electrolytes were synthesized during this study. An anode of commercial Yttria-stabilized zirconia and a cathode of commercial $La_{0.8}Sr_{0.2}MnO_3$ (1.0 μm, Tosho, Japan) were selected. The top and cross-section morphologies of a single cell were evaluated, and the electrochemical properties and the output of an SOFC single cell were measured under optimum conditions.

2. Experimental

2.1. Synthesis of Octahedral-Shaped Ni. The NiO was synthesized by the microwave thermal treatment method. The process used was as follows. First, after the addition of polystyrene (molecular weight = 10,000, Aldrich, USA) and Ni source ($NiCl_2 \cdot H_2O$, 99.95%, Junsei Chemical, Japan) into ethanol, the solution was stirred homogeneously. The mixed solution was then placed in a quartz liner and the solution was microwave heated at 300 W for 15 min. The product like a lump so obtained was then thermally treated at 450°C for 3 h to allow crystallization and remove polymer components. To prepare anode functional layers, we purchased a commercially available YSZ powder (TZ8Y, D50 = 3 μm, Tosoh, Japan). To prepare the synthesized NiO (60 wt%)/YSZ (40 wt%) material, a physically mixing technique was used.

2.2. Characterization of Octahedral-Shaped NiO. The prepared NiO was subjected to powder XRD analysis (model MPD from PANalytical) using nickel-filtered CuKα radiation (30 kV, 30 mA) at 2-theta angles of 10–90. The scan speed was 10°/min, and the time constant was 1 s. The sizes and shapes of microparticles were determined by FE-SEM (field emission scanning electron microscopy, SEM-S-4100, Hitachi) at 120 kV. The morphologies were observed using a scanning electron microscope. Particle sizes were determined using a particle size analyzer (LA-950V2, Horiba, Japan). Zeta potentials were determined by measuring electrophoretic mobility using an electrophoresis measurement apparatus (ELS 8000, Otsuka Electronics, Japan). Electrophoretic light scattering (ELS) determinations were performed in reference beam mode using a laser light source wavelength of 670 nm,

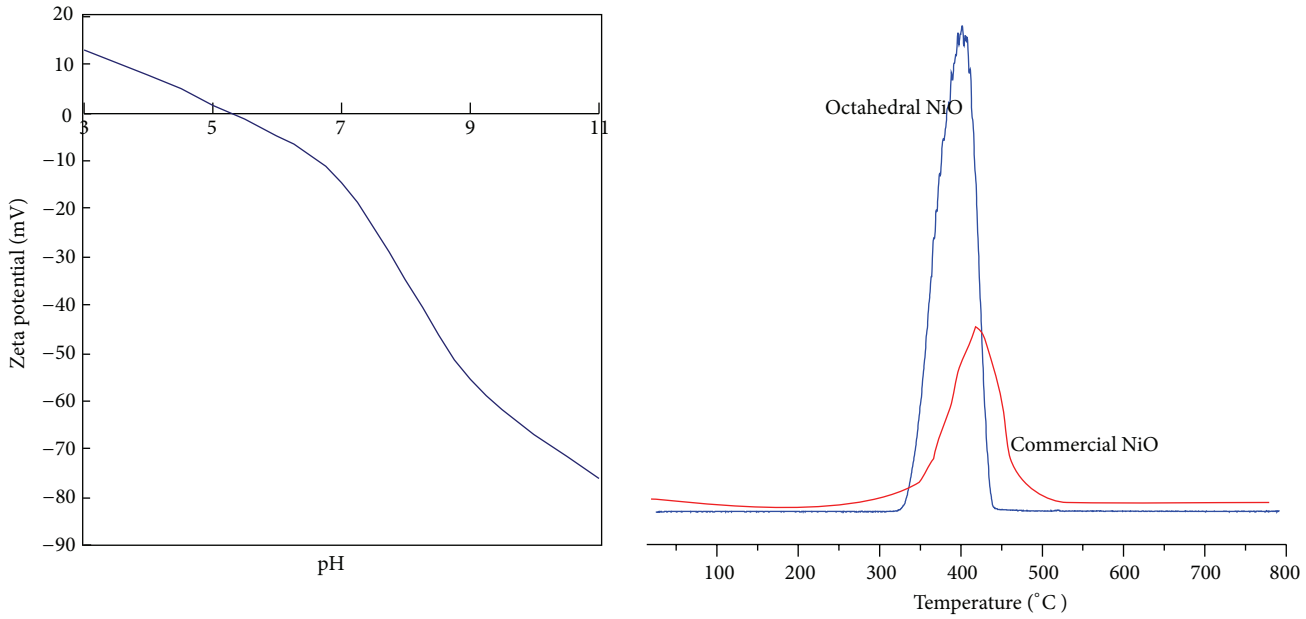

Characteristics/pHs	pH = 3	pH = 5	pH = 7	pH = 9	pH = 11
Zeta potential (mV)	12.91	1.44	−14.56	−55.7	−76.04
Particle size (nm)	8142.8	4996	14220.4	17595	25584.4

FIGURE 2: The zeta potential distribution (a) and H_2-TPR profile (b) of the octahedral NiO sample.

a modular frequency of 250 Hz, and a scattering angle of 15°. The standard errors of the zeta potentials, converted from experimentally determined electrophoretic mobility, were typically <1.5% and percent errors were <5%. To measure zeta potentials, 0.1 wt% NiO was dispersed in deionized water and the pH of the solution was adjusted 3, 5, 7, 9, and 11 with HCl or NaOH. The relative molecular diameter size distributions of the various solutions were also measured using this equipment. Zeta potential distributions were obtained by averaging 2 or 3 runs. H_2-temperature-programmed reduction (TPR) was conducted as follows. About 0.3 g of NiO was pretreated under helium flow (30 mL/min) at 700°C for 2 h and then cooled to room temperature. The analysis was carried out using a thermal gravimetric analyzer at H_2 (10 vol%)/N_2 flow rate of 30 mL/min and by raising the temperature from room temperature to 800°C at 5°C/min.

2.3. Fabrication of Solid Oxide Fuel Cells Using Decalcomania Method. The decalcomania paper was prepared next. Briefly, two types of commercial and synthesized NiO were each mixed with YSZ powders at a weight ratio 6 : 4 in a mortar for 1 h to obtain anode functional layer (AFL) precursor powder. Mixtures were reduced to unique and fine particles (5~10 μm) using a 3-roll ball mill (EXAKT50, German) and a high speed mixer (Thinky centrifugal mixer, Japan), and then a binder (benzene oil) was dropped into the powder mixture (the weight ratio of powder to benzene oil in paste was 58~66 : 42~34). The prepared pastes were assembled onto decalcomania sheets (Tullis Russell Coaters, Republic of Korea) using screen printing equipment (DSP-380VS, Nsys, Republic of Korea). Papers were dried at 40°C for 24 h and then detached from decalcomania sheets to use anode functional layer. First, the AFL layer was fabricated onto a ceramic support (Φ20 mm disk) using the decalcomania coating method and then an electrolyte (YSZ) layer paper was attached to the AFL layer. The layers were pretreated at 400°C for 1 h to remove the organic binder and then cotreated at 1400°C for 10 h at a heating rate of 3°C/min. $La_{0.7}Sr_{0.3}MnO_3$/YSZ paper cathode was fabricated on the YSZ films using the decalcomania method. Finally, the assembled cell was sintered by heating at 1200°C for 2 h. Cell 1 was based on commercial NiO anodes (particle size 0.6 μm, Sumitomo, Japan) and NiO anode in cell 2 was synthesized in this study; cell efficiencies were compared. Pt paste (DAD-87, China) was employed as a current collector and a sealing material. After being sealed, cells were tested for power density in an electrical furnace using the four-probe method. The NiO/YSZ anode was reduced in situ at 800°C. The anode was fed with hydrogen at a flow rate of 500 mL min^{-1} and the cathode was exposed to an oxygen flow of 1,000 mL min^{-1}. *I-V* characteristics and ELS impedance spectra were measured using an SOFC Button Cell Test Station (Nara Cell Tech., Republic of Korea) and an impedance analyzer SI 1260 (Solatron, England) at a frequency range of 1 Hz to 100,000 Hz and at an AC voltage of 20 mV.

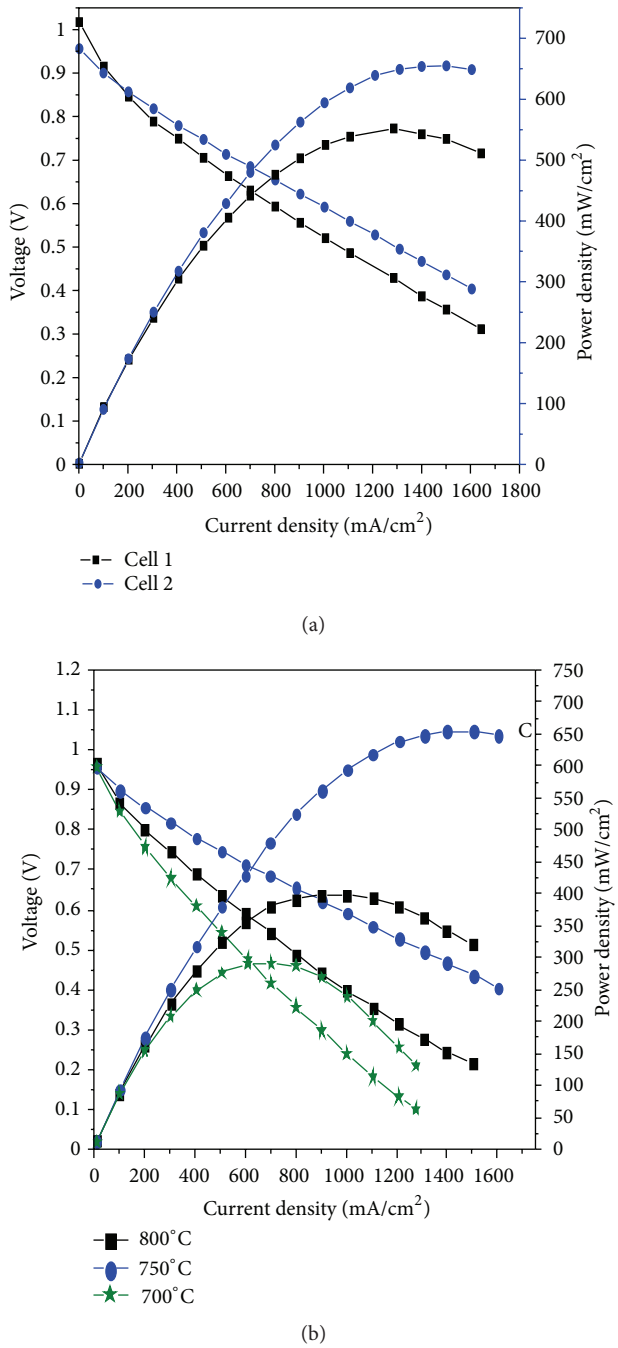

FIGURE 3: The *I-V* and power density curves of single cells based on commercial NiO and synthesized octahedral NiO anode functional layers (a) at different temperatures (b).

3. Results and Discussion

Figures 1(a), 1(b), and 1(c) show the XRD pattern, SEM image, and particle size distribution of an NiO powder synthesized by microwave treatment. We believe in the microwave chamber that ROR or H_2O elimination rapidly induces a combination between each Ni alkoxide or hydroxide. During this reaction, the condensation reaction continues in the absence of any blocking molecules, and the resulting nucleated NiO can grow in all directions to produce a spherical-shaped NiO. However, the presence of polystyrene induces a selective and competitive condensation reaction at the six terminals of the Ni hydroxide complexes, resulting in an octahedral shape. These results revealed that microwave pretreatment had a significant effect on crystal growth, presumably because microwave treatment processing induces rapid hydrolysis of Ni–OH or Ni–OR and polycondensation of these. Initial growth leads to a linear chain of Ni–OH and the high concentration of OH ions present leads to crystallization of NiO possibly because the intermolecular reaction between each Ni–OH is higher than the intra-molecular reaction. Due to the complexity of the NiO synthetic method, perfect octahedral NiO has not been synthesized for SOFCs. Fortunately, we were able to obtain the octahedral NiO by using the microwave thermal treatment method, as shown in Figure 1(a). The NiO structure showed peaks at 2 theta = 38.0, 43.5, 63.0, 70.0, and 78.58, which were assigned to the (d111), (d200), (d220), (d311), and (d222) planes, respectively [19]. Line broadening of the peak of the main 200 plane is related to crystallite size. The full width at half maximum (FWHM) of the peak at 2 theta = 43.58 was estimated using Scherrer's equation [20] ($t = 0.9\lambda/\beta \cos\theta$, where λ is the wavelength of incident X-rays, β the FWHM height in radians, and θ the diffraction angle). From this calculation, the crystalline domain size was calculated as 7.2 μm. Figure 1(b) shows FE-SEM images of the particle shapes of NiO. A relatively uniform octahedral shape and particle sizes in the range 4~10 μm (average size 7.2 μm by the particle size analyzer in Figure 1(c)) were observed.

Figures 2(a) and 2(b) depict the influence of pH on the position of the zeta potential distribution and H_2-TPR profile of the octahedral NiO sample. Aggregated particle sizes in aqueous solution are summarized in the table in Figure 2. The zeta potentials of octahedral NiO suspensions significantly decreased on increasing pH (Figure 2(a)). Surface charges changed from positive in acidic solution to negative in alkali solution. The isoelectric point was at pH 5.4 and at this value a large amount of aggregation occurred. Absolute surface charge peaked at −76.04 mV at pH 11, indicating that the octahedral colloidal NiO is stable [21]. At this level, it exhibited little aggregation, indicating that reaction sites were present over the surface of the anode material. In addition, we compared the H_2-TPR profiles of the two NiO samples (octahedral and commercial), as shown in Figure 2(b). One H_2-TPR peak corresponding to the reduction of the NiO component was observed. In general, H_2-TPR results indicated that (1) the peak area corresponded to hydrogen uptake and (2) the peak at high temperatures corresponded to the chemical reduction. The reduction peaks of the octahedral NiO sample were gradually shifted more so to lower temperatures than those of the commercial NiO. Ni^{2+} ions were reduced to Ni^0 at a comparatively low temperature of 330~430°C in octahedral NiO.

Figures 3(a) and 2(b) compare the *I-V* and power density curves of a single cell based on commercial NiO (cell 1) and the cell assembled by synthesized octahedral NiO anode functional layers (cell 2). Maximum power densities

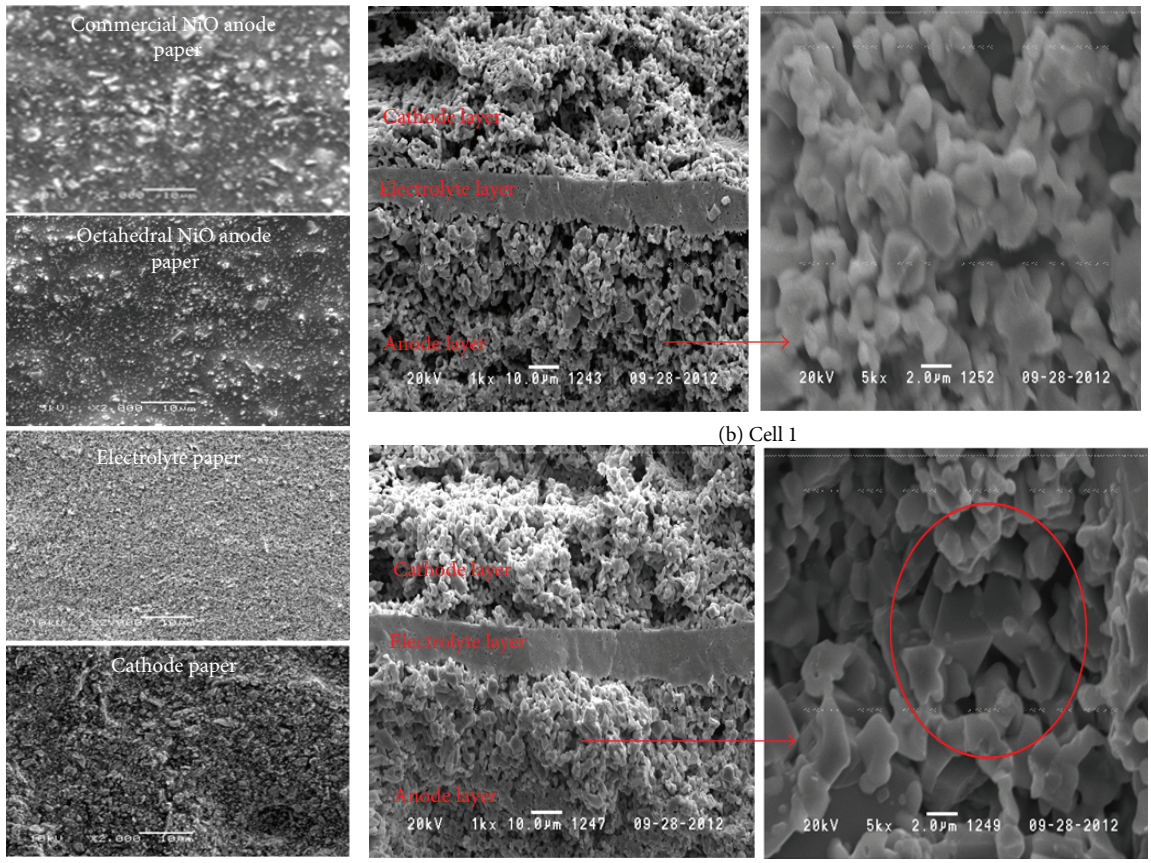

Figure 4: FE-SEM micrographs of cells with different anode functional layers after SOFC testing.

in cells 1 and 2 were measured at 551 and 654 mWcm^{-2} at 800°C, respectively (Figure 3(b)). Cell performance was significantly improved by the addition of the octahedral NiO anode functional layer. In Figure 3(b), according to operating temperatures, the maximum power densities on a single type of cell were increased up to 293, 401, and 654 mW cm^{-2} at 700, 750, and 800°C, respectively.

We considered that fuel cell performance differences could be due to different interfacial microstructures.

Figures 4(a) and 4(b) show the SEM micrographs of the cells with different anode functional layers after SOFC testing. The pores in the commercial NiO-AFL (cell 1) are submicron in diameter and the large pores are 2~5 micrometers in diameter. The estimated porosity of the commercial AFL is about 35%. However, the pores in the octahedral NiO-AFL (cell 2) were smaller than those in commercial NiO-AFL. Large cracks were clearly discernible at the interface between the AFL and the electrolyte layer in the commercial NiO cell, but no crack was observed in the octahedral NiO cell. The development of cracks at the AFL/electrolyte layer interface was probably caused by the differential sintering shrinkages of the multiple layers, and thus, the octahedral NiO particles perhaps better matched the YSZ electrolyte particles in this respect. Additionally the grains between octahedral NiO particles were well connected in octahedral NiO-AFL cells.

Fewer cracks at the AFL/electrolyte interface result in a lower ohmic cell ASR. Electrochemical impedance spectroscopy (EIS) measurements in open-circuit conditions were used to evaluate the resistance values with respect to operating temperature for the octahedral NiO-AFL cell. Figure 5 shows typical Nyquist plots of cells with an octahedral NiO anode functional layer, measured at 700, 750, and 800°C. The intercept with the real axis at high frequency represents the ohmic resistance of a cell (Rohmic), which includes its electrolyte and lead wire resistances and some contact resistance associated with interfaces. The low-frequency intercept corresponds to the total resistance of the cell. Therefore, the difference between the high frequency and low frequency represents the total interfacial polarization resistance (R_p) of the cell [22]. The Rohmic of the cell was almost the same (0.78 Ω cm^{-2}) at all temperatures, but R_p was significantly lower at 800°C than at 700 and 750°C. R_p reduced from 2.85 to 1.21 Ω cm^{-2}, respectively, with increasing temperature from 700 to 850°C. Generally, these different resistance values are ascribed to the addition of the anode functional layer, since other parameters, such as electrolyte thickness, cathode material, anode substrate, and sintering temperature, were kept constant. As mentioned above, R_p is mainly due to electrolyte and contact resistance. Therefore, a better contact between electrolyte and anode can decrease contact resistance and

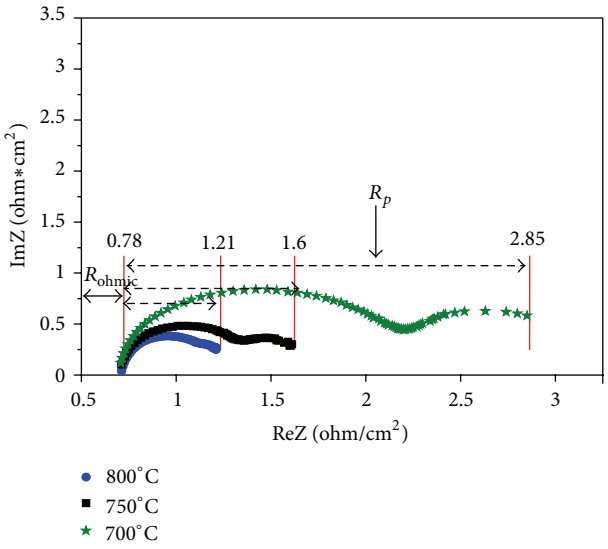

Figure 5: Typical Nyquist plots of cells with an octahedral NiO anode functional layer at 700, 750, and 800°C.

reduce total R_p for a given electrolyte thickness. At the anode/electrolyte interface for the cell with anode functional layer, the elimination of macropores led to a better contact between electrolyte and the anode, which reduced contact resistance at the anode/electrolyte interface. In this study, the octahedral NiO-AFL cell provided lower R_p values due to faster electrochemical reactions at the anode/electrolyte interface.

4. Conclusions

This study described the effect of anode functional layer on SOFC performance. Identical single cells, differing only in terms of anode functional layer morphology, were fabricated and tested. Using an octahedral NiO anode functional layer, fuel cell performance was significantly improved by up to a power output of 100 mWcm^{-2} at 850°C, due to better contact between the electrolyte and anode. These findings demonstrate cell performance is critically dependent on anode microstructure and that microwave thermal treatment provides an effective means of octahedral NiO anode materials.

Acknowledgments

This work was supported by the New & Renewable Energy of the Korea Institute of Energy Technology Evaluation and Planning (KETEP) Grant funded by the Korea Government Ministry of Knowledge Economy (no. 2010T100100622).

References

[1] T. Suzuki, Y. Funahashi, T. Yamaguchi, Y. Fujishiro, and M. Awano, "Development of cube-type SOFC stacks using anode-supported tubular cells," *Journal of Power Sources*, vol. 175, no. 1, pp. 68–74, 2008.

[2] T. Yamaguchi, S. Shimizu, T. Suzuki, Y. Fujishiro, and M. Awano, "Fabrication and evaluation of a novel cathode-supported honeycomb SOFC stack," *Materials Letters*, vol. 63, no. 29, pp. 2577–2580, 2009.

[3] Y. Yang, G. Wang, H. Zhang, and W. Xia, "Computational analysis of thermo-fluid and electrochemical characteristics of MOLB-type SOFC stacks," *Journal of Power Sources*, vol. 173, no. 1, pp. 233–239, 2007.

[4] F. Smeacetto, M. Salvo, M. Santarelli et al., "Performance of a glass-ceramic sealant in a SOFC short stack," *International Journal of Hydrogen Energy*, vol. 38, no. 1, pp. 588–596, 2013.

[5] M. Lockett, M. J. H. Simmons, and K. Kendall, "CFD to predict temperature profile for scale up of micro-tubular SOFC stacks," *Journal of Power Sources*, vol. 131, no. 1-2, pp. 243–246, 2004.

[6] F. Tietz, H. P. Buchkremer, and D. Stöver, "Components manufacturing for solid oxide fuel cells," *Solid State Ionics*, vol. 152-153, pp. 373–381, 2002.

[7] J. Will, A. Mitterdorfer, C. Kleinlogel, D. Perednis, and L. J. Gauckler, "Fabrication of thin electrolytes for second-generation solid oxide fuel cells," *Solid State Ionics*, vol. 131, no. 1, pp. 79–96, 2000.

[8] D. Rui, H. Zhang, G. Wang, F. Xiong, and B. Hu, "Fabrication of finely structured silicon-supported SOFC with anode deposited by multi-phase plasma spraying," *Journal of Materials Processing Technology*, vol. 212, pp. 2193–2199, 2012.

[9] Y. C. Yang, T. H. Chang, Y. C. Wu, and S. F. Wang, "Porous Ni/8YSZ anode of SOFC fabricated by the plasma sprayed method," *International Journal of Hydrogen Energy*, vol. 37, pp. 13746–13754, 2012.

[10] L. R. Pederson, P. Singh, and X. D. Zhou, "Application of vacuum deposition methods to solid oxide fuel cells," *Vacuum*, vol. 80, no. 10, pp. 1066–1083, 2006.

[11] Y. Du, N. M. Sammes, and G. A. Tompsett, "Optimisation parameters for the extrusion of thin YSZ tubes for SOFC electrolytes," *Journal of the European Ceramic Society*, vol. 20, no. 7, pp. 959–965, 2000.

[12] Q. Yang, J. Sha, X. Ma, and D. Yang, "Synthesis of NiO nanowires by a sol-gel process," *Materials Letters*, vol. 59, no. 14-15, pp. 1967–1970, 2005.

[13] C. Zhang, J. Zhan, J. Wu, X. Guo, and M. Okido, "Preparation of fibrous nickel oxide particles," *Transactions of Nonferrous Metals Society of China*, vol. 13, pp. 1441–1445, 2003.

[14] S. M. Tan, S. P. Chai, W. W. Liu, and A. R. Mohamed, "Effects of FeO_x, CoO_x, and NiO catalysts and calcination temperatures on the synthesis of single-walled carbon nanotubes through chemical vapor deposition of methane," *Journal of Alloys and Compounds*, vol. 477, no. 1-2, pp. 785–788, 2009.

[15] A. M. Reddy, A. S. Reddy, K. S. Lee, and P. S. Reddy, "Growth and characterization of NiO thin films prepared by dc reactive magnetron sputtering," *Solid State Sciences*, vol. 13, no. 2, pp. 314–320, 2011.

[16] C. H. Jung, S. Jalota, and S. B. Bhaduri, "Quantitative effects of fuel on the synthesis of Ni/NiO particles using a microwave-induced solution combustion synthesis in air atmosphere," *Materials Letters*, vol. 59, no. 19-20, pp. 2426–2432, 2005.

[17] F. Rousseau, S. Awamat, M. Nikravech, D. Morvan, and J. Amouroux, "Deposit of dense YSZ electrolyte and porous NiO-YSZ anode for SOFC device by a low pressure plasma process," *Surface and Coatings Technology*, vol. 202, no. 4–7, pp. 1226–1230, 2007.

[18] S. Biswas, T. Nithyanantham, S. N. Thangavel, and S. Bandopadhyay, "High-temperature mechanical properties of reduced NiO-8YSZ anode-supported bi-layer SOFC structures in ambient air and reducing environments," *Ceramics International*, vol. 39, no. 3, pp. 3103–3111, 2013.

[19] D. Y. Han, H. Y. Yang, C. B. Shen, X. Zhou, and F. H. Wang, "Synthesis and size control of NiO nanoparticles by water-in-oil microemulsion," *Powder Technology*, vol. 147, no. 1–3, pp. 113–116, 2004.

[20] N. M. Deraz, M. M. Selim, and M. Ramadan, "Processing and properties of nanocrystalline Ni and NiO catalysts," *Materials Chemistry and Physics*, vol. 113, no. 1, pp. 269–275, 2009.

[21] L. Zhang, S. P. Jiang, W. Wang, and Y. Zhang, "NiO/YSZ, anode-supported, thin-electrolyte, solid oxide fuel cells fabricated by gel casting," *Journal of Power Sources*, vol. 170, no. 1, pp. 55–60, 2007.

[22] Q. L. Liu, K. A. Khor, and S. H. Chan, "High-performance low-temperature solid oxide fuel cell with novel BSCF cathode," *Journal of Power Sources*, vol. 161, no. 1, pp. 123–128, 2006.